Band structure and superconductivity in twisted trilayer graphene

Võ Tiến Phong, Pierre A. Pantaleón, Tommaso Cea, and Francisco Guinea

Phys. Rev. B **104**, L121116 — Published 27 September 2021

DOI: 10.1103/PhysRevB.104.L121116

Band Structure and Superconductivity in Twisted Trilayer Graphene

VÕẹ Tiòểỉn Phong,[1] Pierre A. Pantaleón,[2] Tommaso Cea,[2] and Francisco Guinea[2,3]

[1]*Department of Physics and Astronomy, University of Pennsylvania, Philadelphia PA 19104*
[2]*Imdea Nanoscience, Faraday 9, 28015 Madrid, Spain*
[3]*Donostia International Physics Center, Paseo Manuel de Lardizábal 4, 20018 San Sebastián, Spain*

(Dated: July 8, 2021)

We study the symmetries of twisted trilayer graphene's band structure under various extrinsic perturbations, and analyze the role of long-range electron-electron interactions near the first magic angle. The electronic structure is modified by these interactions in a similar way to twisted bilayer graphene. We analyze electron pairing due to long-wavelength charge fluctuations, which are coupled among themselves via the Coulomb interaction and additionally mediated by longitudinal acoustic phonons. We find superconducting phases with either spin singlet/valley triplet or spin triplet/valley singlet symmetry, with critical temperatures up to a few Kelvin for realistic choices of parameters.

Introduction: Recently, it has been shown that superconductivity and exotic correlated phases can emerge when two or three monolayers of graphene are laterally stacked with a small relative twist angle between successive layers [1–4]. Observation of insulating behavior and/or superconductivity have also been reported for graphene bilayers on hBN substrates [5, 6], ABC-stacked trilayers on hBN substrates [7–10], pairs of graphene bilayers twisted with respect to each other [11–14], rhombohedral tetralayers [15], rhombohedral trilayers [16, 17] and twisted transition-metal-dichalcogenide layers [18]. However, twisted bilayer graphene (TBG) [1, 2] and its recent cousin, the alternating-angle twisted trilayer graphene (TTG) [3, 4], are the only systems to date where superconductivity has been unambiguously established [19–21].

Twisted trilayer graphene with alternating angles shows a series of magic angles with remarkably flat bands, where, under certain conditions, the trilayer system behaves as a TBG with renormalized interlayer hoppings plus a monolayer [22]. This follows from the mirror symmetry around the central layer of the system. This symmetry can be broken by various experimentally-relevant perturbations. In this case, calculations of the electronic structure in the absence of this mirror symmetry shows hybridized monolayer and twisted bilayer features [3, 23–27]. The effects of electron-electron interactions and spin fluctuations have also been considered [24–31], as well as the role of external magnetic fields [32].

In this work, we study the symmetries of the continuum model, the effects of symmetry-breaking perturbations on the band structure, and the renormalization of electronic energies by electron-electron interactions within a self-consistent Hartree formalism, complemented by the analysis of the exchange potential at half filling. Then by using an extended Kohn-Luttinger mechanism that includes electron-hole pairs, plasmons, and phonons, we analyze how the screened Coulomb interaction can induce pairing in TTG.

Band structure and symmetries of the continuum model: To form TTG, we consider three monolayers stacked one on top of the other in perfect atomic registry, i.e. in the AA stacking configuration. Labeling the layers consecutively, we twist layers $\ell = 1$ and $\ell = 3$ by $-\theta/2$ and layer $\ell = 2$ by $+\theta/2$ about a fixed hexagon center. To describe the low-energy physics at small angles, we adopt a valley-projected continuum Hamiltonian [22, 33–35]

$$\begin{aligned}
\mathcal{H}^{\theta}_{\nu}(\mathbf{k},\mathbf{r}) &= \begin{pmatrix} \mathfrak{h}_{\nu}\left(\mathbf{k}^{+\frac{\theta}{2}}\right)+V_1 & \left[\mathfrak{t}^{\theta}_{\nu}(\mathbf{r})\right]^{\dagger} & \mathfrak{t}_{\mathrm{AA}} \\ \mathfrak{t}^{\theta}_{\nu}(\mathbf{r}) & \mathfrak{h}_{\nu}\left(\mathbf{k}^{-\frac{\theta}{2}}\right) & \mathfrak{t}^{\theta}_{\nu}(\mathbf{r}) \\ \mathfrak{t}^{\dagger}_{\mathrm{AA}} & \left[\mathfrak{t}^{\theta}_{\nu}(\mathbf{r})\right]^{\dagger} & \mathfrak{h}_{\nu}\left(\mathbf{k}^{+\frac{\theta}{2}}\right)+V_3 \end{pmatrix}, \\
\mathfrak{h}_{\nu}(\mathbf{k}) &= -\hbar v_F\left(\mathbf{k}-\mathbf{K}_{\nu}\right)\left(\nu\sigma_x,\sigma_y\right), \\
\mathfrak{t}^{\theta}_{\nu}(\mathbf{r}) &= \begin{pmatrix} w_0 & w_1 \\ w_1 & w_0 \end{pmatrix} + \begin{pmatrix} w_0 & w_1 e^{-i\phi} \\ w_1 e^{i\phi} & w_0 \end{pmatrix} e^{i\nu\mathbf{G}^{\mathrm{M}}_1\cdot\mathbf{r}} \\
&\quad + \begin{pmatrix} w_0 & w_1 e^{i\phi} \\ w_1 e^{-i\phi} & w_0 \end{pmatrix} e^{i\nu\left(\mathbf{G}^{\mathrm{M}}_1+\mathbf{G}^{\mathrm{M}}_2\right)\cdot\mathbf{r}}, \\
\mathfrak{t}_{\mathrm{AA}} &= \begin{pmatrix} \gamma_2 & 0 \\ 0 & \gamma_2 \end{pmatrix},
\end{aligned} \tag{1}$$

where $\phi = 2\pi\nu/3$, $\hbar v_F/a = 2.135$ eV, $w_0 = 79.7$ meV and $w_1 = 97.5$ meV are the interlayer tunneling amplitudes whose imbalance accounts for some lattice relaxation [34], $\nu = \pm$ is the valley index, $\mathbf{k}^{\theta} = R(\theta)\mathbf{k}$, $\mathbf{K}_{\pm} = \frac{4\pi}{3a}(\mp 1, 0)$ are the microscopic unrotated zone corners, and γ_2 is a small AA coupling between the first and third layers. If we use the conventional Slater-Koster parametrization [34], $\gamma_2 \approx 0.3$ meV, which justifies its neglect hereafter. It is included here to clarify some symmetry properties to be discussed. We note in passing that this approximation warrants further inspection in future work since it plays an important role in the modeling of graphite's band structure [36, 37]. To study various perturbations [38–42], we also add on-site couplings to the first and third layers. For substrate induced masses, $V_1 = \delta_1\sigma_z, V_3 = \delta_3\sigma_z$, while for a perpendicular displacement field, $V_1, V_3 \propto \mathbb{1}$. Direct coupling to $\ell = 2$ is ignored since this layer is encapsulated and therefore difficult to access.

We now consider the symmetries of Hamiltonian (1) with $V_1 = V_3 = 0$. Our choice of twist center ensures that the structure is maximally symmetric. A different

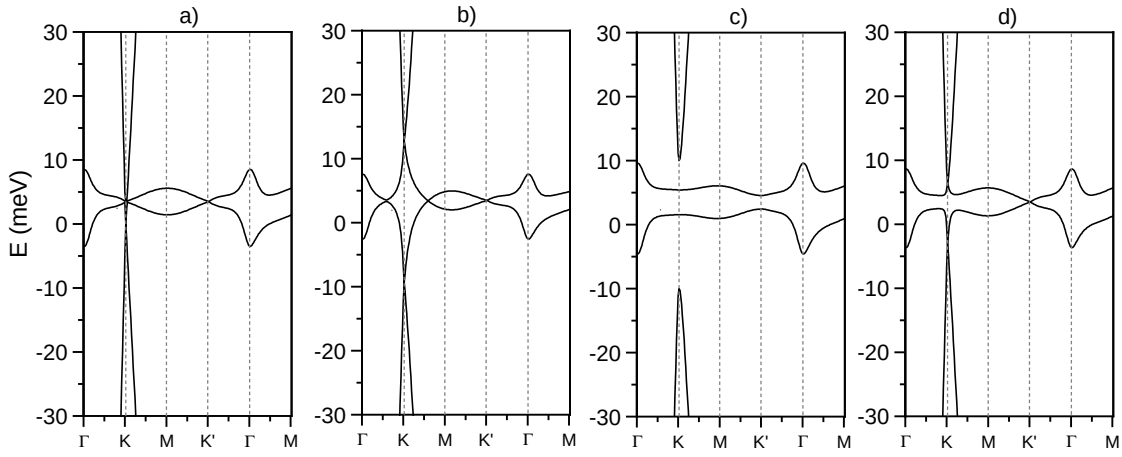

Figure 1. **Single-particle band structure with various perturbations:** (a) Intrinsic TTG with a twist angle of $\theta = 1.59°$ where the monolayer band is decoupled from the narrow bilayer bands. (b) A perpendicular displacement field $\Delta V = 50$ meV between the outermost layers hybridizes these bands. (c) A non-zero staggered sublattice potential, $\delta_1 = \delta_3 = 10$ meV, generically breaks both $\mathcal{T}C_{2z}$ and M_z and gaps out the Dirac cones near charge neutrality, endowing the resulting bands with possible nonzero Chern numbers. (d) For the special case, $\delta_1 = -\delta_3$, while both $\mathcal{T}C_{2z}$ and M_z are broken individually, $\mathcal{T}C_{2z}M_z$ is preserved. In this case, we find that the bands are mixed, but the Dirac cones are preserved, though they can be pushed to different energies.

twist center, for instance, about a registered site, retains only a subgroup of the maximal group. The vertical rotations about the z axis, C_{6z}, are respected by each plane individually. The horizontal rotations about the in-plane axes, C_{2x} and C_{2y}, preserved by TBG, are explicitly broken due to the presence of the middle layer in TTG. However, reflection symmetry about the plane of the middle layer M_z that exchange the top and bottom layers is preserved in TTG. Alternatively, one can substitute M_z for inversion symmetry $\mathcal{I}$ that is equivalent to M_z followed by a rotation. Therefore, the point symmetry group of the lattice is $C_{6h} \otimes \mathcal{T}$, where $\mathcal{T}$ is local time-reversal symmetry. In addition to these microscopic point symmetries, we can also now impose valley projection symmetry which becomes exact in the limit of large moiré wavelength. In this case, only a subset of $C_{6h} \otimes \mathcal{T}$ is preserved at a single valley, namely C_{2z} is broken because it takes $\mathbf{K}_+$ to $\mathbf{K}_-$ in momentum space. The symmetry group of the Hamiltonian thus factorizes into a direct product of valley symmetry and a magnetic point symmetry group that consists of $\{C_{3z}, \mathcal{T}C_{2z}, M_z\}$.

The presence of z-mirror symmetry allows us to simplify Eq. (1) significantly. Mirror symmetry maps the middle layer, $\ell = 2$, into itself, while it interchanges layers $\ell = 1$ and $\ell = 3$. So we can form linear combinations of the wavefunctions of these two exchanged layers that are odd and even under mirror symmetry. Such a transformation is executed by the unitary operator $\mathcal{U} = 2^{-1}\left(1, 0, 1; 0, \sqrt{2}, 0; -1, 0, 1\right)$ [22, 35]. Under this transformation, the Hamiltonian factorizes into $\tilde{\mathcal{H}}^{\theta}_{\nu}(\mathbf{k}, \mathbf{r}) = \mathcal{U}\mathcal{H}^{\theta}_{\nu}(\mathbf{k}, \mathbf{r})\mathcal{U}^{\dagger} = \tilde{\mathcal{H}}^{\theta,\nu}_{\mathrm{TBG}}(\mathbf{k}, \mathbf{r}) \oplus \tilde{\mathcal{H}}^{\theta,\nu}_{\mathrm{MLG}}(\mathbf{k})$, where the mirror-odd sector, $\tilde{\mathcal{H}}^{\theta,\nu}_{\mathrm{TBG}}(\mathbf{k}, \mathbf{r})$, behaves as though it were a TBG system with enhanced interlayer couplings by a factor of $\sqrt{2}$ and the mirror-even sector, $\tilde{\mathcal{H}}^{\theta,\nu}_{\mathrm{MLG}}(\mathbf{k}, \mathbf{r})$, mimics a single rotated layer of graphene. $\mathfrak{t}_{\mathrm{AA}}$ behaves like an interlayer bias on the bilayer spectrum, and an overall shift in the monolayer spectrum. This transformation is convenient because it casts the Hamiltonian into a direct sum of two Hamiltonians that are well-understood. Denoting operators in the new basis with an overline tilde, we see that $\tilde{C}_{3z} = C_{3z}$ and $\tilde{\mathcal{T}}\tilde{C}_{2z} = \mathcal{T}C_{2z}$ since these preserve layer index. In the mirror-odd sector, there are additional symmetries thus far neglected that exchange the mirror basis states when $\gamma_2 = 0$. We can call them $\tilde{C}_{2x}$ and $\mathcal{T}\tilde{C}_{2y}$, although they do not correspond naturally to rotations in the original layer basis. When $\gamma_2 \neq 0$, these symmetries are broken, but all the other symmetries of the lattice in the layer basis are still preserved.

Within a single valley, we have one unbounded Dirac cone coming from the monolayer spectrum located at either K or K'; in addition, we also have two Dirac cones at K and K' from the TBG's flat bands near charge neutrality. These Dirac cones are protected by $\mathcal{T}C_{2z}$ as in TBG [43, 44]. The two Dirac cones from the TBG spectrum are related to each other by $\tilde{C}_{2x}$, and consequently, are pinned to the same energy. However, in the absence of particle-hole symmetry, there is no symmetry which pins the monolayer Dirac cone to the same energy. Because of this energy offset, unlike in TBG, TTG in the single-particle limit is formally metallic for all energies in the continuum model. This important difference alters the Fermi surface geometry of TTG when compared to TBG, and may be important in the analysis of correlated insulating phases. For instance, there is technically no magic angle around which isolated energy bands become

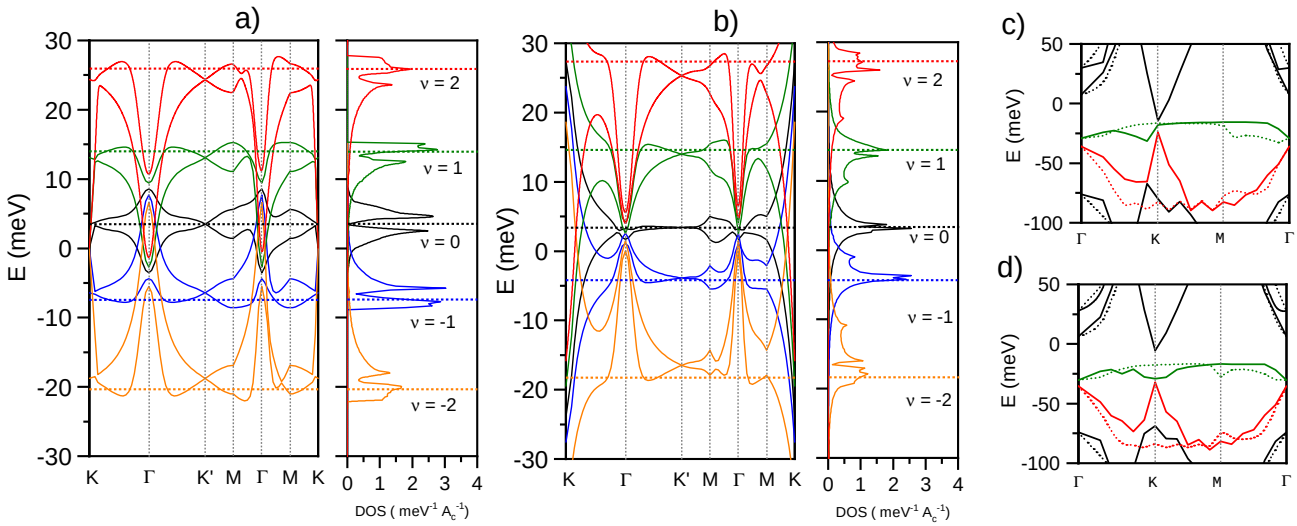

Figure 2. **Hartree-Fock renormalization of band structure:** Low energy band structure and DOS obtained for $\theta = 1.59°$ with (a) $\Delta V = 0$ meV and (b) $\Delta V = 60$ meV. Different colors denote different fillings, as indicated in the DOS. The horizontal lines denote the Fermi level. The Fock bands at half filling are shown in for (c) $\Delta V = 0$ and (d) $\Delta V = 50$ meV. Dotted lines are the bands in the opposite valley.

spectrally flatten like in TBG. However, the presence of z-mirror symmetry allows us to still define a quasi-flat band by first projecting into the mirror-odd sector and then imposing band-flatting conditions on just the two bands nearest to charge neutrality within this sector. The highly-dispersive monolayer band becomes a spectator in this scheme. For our choice of parameters, this scheme produces a magic angle at $\theta \approx 1.57°$. This magic angle occurs at a larger angle than in TBG because of the enhancement in interlayer coupling strengths. In addition, we can also add an interlayer bias that couples directly to the $\ell = 1$ and $\ell = 3$ layers. The presence of this potential preserves all in-plane symmetries, but it breaks M_z. Because of this, the monolayer and bilayer bands are hybridized. However, in this case, the Dirac cones that are protected by in-plane symmetries are maintained; secondary Dirac points can be generated as well. To liberate these Dirac cones, we can add staggered sublattice potentials to the outer layers. Generically, this breaks both M_z and C_{2z} symmetries, and therefore, can gap out the Dirac cones as well as hybridizing the mirror-odd and mirror-even sectors.

Band structures for different sets of parameters are shown in Fig. 1. In Fig. 1a, we observe that pristine TTG features decoupled bands from the mirror-odd and mirror-even sectors. A perpendicular displacement field $\Delta V = V_1 - V_3$ couples these two sectors, as shown in Fig. 1b. The presence of a substrate induces an staggered sublattice potential that can couple the two mirror sectors as well as gapping out all the Dirac cones in the system, as shown in Fig. 1c. In this situation, the narrow bands are isolated from all the other bands and can carry a finite Berry curvature. Depending on the value of the staggered sublattice potential, the Chern topology of these bands can be tuned, as detailed in Ref. [45].

Long-range Coulomb interaction: At fractional fillings, interaction-driven band renormalization can significantly distort the bands represented in Fig. 1. We now consider the effect of the long range Coulomb interaction treated within the self-consistent Hartree-Fock approximation in Eq (1). As emphasized in Refs. [46–48] the inhomogeneous charge distribution leads to an electrostatic potential of the order of $V_0 \sim e^2/\epsilon L$, where e is the electron charge and L the moiré length. In TBG near the magic angle, it has been shown that the electrostatic Hartree interaction strongly distorts the band structure [47]. In TTG, the situation is quite similar; we find that the self-consistent order parameter of the Hartree Hamiltonian also depends linearly on the filling fraction owing to the dominance of the narrow bands over the monolayer Dirac cones. Figure 2 displays the band structure of TTG as a function of filling for a screening of $\epsilon = 10$. The effect of the Hartree potential varies significantly as a function of filling. This leads to an approximate pinning of the van Hove singularities at the Fermi energy at certain fillings, even in the presence of a displacement field.

We also consider the Fock potential. In TBG, this term leads to gaps and broken symmetry phases [48]. We analyze the system at half filling, where the Hartree potential is expected to vanish. The calculations have been carried out by projecting the Fock potential on six central bands [49]. Results are shown in Fig. 2. The non-interacting flat bands are shifted downwards, and significantly widened and separated. The monolayer band is less affected, and the system remains metallic.

Superconductivity: Next, we study the onset of the superconducting (SC) order in TTG, as induced by the combined effects of the 2D plasmon and the longitudinal

acoustic phonons of the three constituting layers. The calculation represents a straightforward generalization of the one developed by two of us in the recent paper [50] for the case of the TBG. It consists in solving the linearized gap equation in which the pairing interaction is mediated by the Coulomb potential screened by the particle-hole excitations and the acoustic phonons within the random phase approximation (RPA). The idea strictly recalls the Kohn-Luttinger mechanism of the superconductivity induced by repulsive interactions [51].

The linearized gap equation can be written as:

$$\tilde{\Delta}^{m_1 m_2}_{\alpha\beta}(\boldsymbol{k}) = \sum_{n_1 n_2} \sum_{\boldsymbol{q}} \Gamma^{m_1 m_2}_{n_1 n_2;\alpha\beta}(\boldsymbol{k},\boldsymbol{q}) \tilde{\Delta}^{n_1 n_2}_{\alpha\beta}(\boldsymbol{q}), \qquad (2)$$

where $\tilde{\Delta}$ is the order parameter, $m_{1,2}, n_{1,2}$ are band indices, α, β are the spin/valley flavors, and Γ is the pairing interaction kernel, which encodes the screened potential as well the temperature dependence of the Eq. (2). A detailed description of the method including the derivation of the Eq. (2) is provided in Ref. [45]. In what follows, we consider inter-valley superconductivity, meaning that α and β have opposite valley indices in the Eq. (2). In contrast, we do not impose any constraint to the spin texture of the SC ground state, meaning that our model can be compatible with both spin singlet or spin triplet superconductivity. However, it is worth noting that the violation of the Pauli limit reported by the recent experiment [52] strongly suggests that the SC ground state of the TTG is a spin triplet.

Given the temperature dependence of the kernel Γ, Eq. (2) defines the SC critical temperature, T_c, as the one at which the largest eigenvalue of Γ is equal to 1. Fig. 3 shows the critical temperature as a function of the filling, ν, obtained for the twist angle $\theta = 1.59°$ and inter-layer potential: $\Delta V = 0$eV (red line) and $\Delta V = 0.06$eV (blue line). The corresponding band structure and density of states (DOS) of the central bands are shown in the Fig. 2. Here, the DOS is expressed in units of meV$^{-1}A_C^{-1}$, A_C being the area of the moiré unit cell. As is evident, the behavior of T_c upon varying the filling follows the evolution of the DOS at the Fermi level, the latter being marked by the horizontal lines.

Finally, we study the symmetry of the SC order parameter, as given by the eigenvector of the kernel Γ, Eq. (2), corresponding to the eigenvalue 1, at $T = T_c$. As a representative case, Fig. 3 shows the amplitude (a) and the phase (b) of the order parameter, in the valence v and conduction c band, as obtained for: $\theta = 1.59°$, $\Delta V = 0.06$eV and $n = -1$. The black lines identify the Fermi surface. Remarkably, also the conduction band contributes to the superconductivity, albeit marginally. The reason for that can be understood by noting that the conduction band crosses the Fermi surface close to the Dirac points, see Fig. 2(b), where the bands flatten. The results of Fig. 3 suggest an extended s-wave symmetry without sign changes along the Fermi surface, which is analogous to what obtained in the Ref. [50] for the case of the TBG.

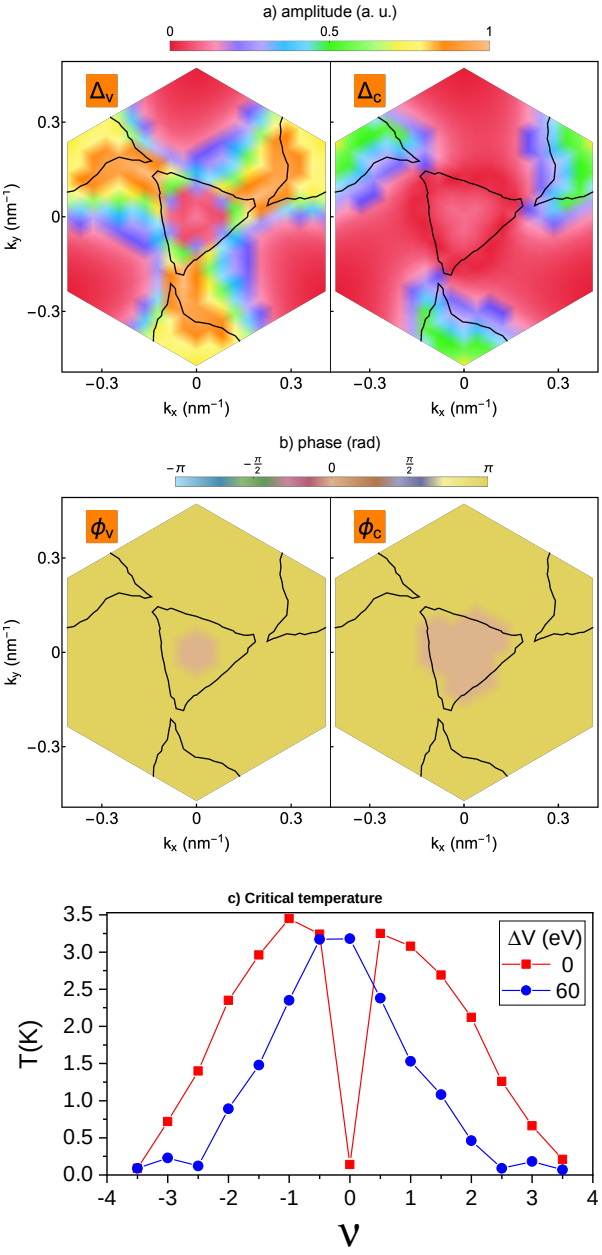

Figure 3. **Superconducting order parameter and transition temperature.** Amplitude (a) and phase (b) of the SC order parameter in the valence v and conduction c band, as obtained for: $\theta = 1.59°$, $\Delta V = 60$ meV and $\nu = -1$. The black lines identify the Fermi surface. c) Critical temperature as a function of the filling, ν, obtained for the twist angle $\theta = 1.59°$ and inter-layer potential: $\Delta V = 0$ meV (red line) and $\Delta V = 60$ meV (blue line).

Conclusions: We have analyzed the symmetries, band structure, role of interactions, and superconductivity of twisted trilayer graphene near the first magic angle. Our results are similar to those found for twisted bilayer graphene. The presence of an additional layer, and the accompanying electronic bands with monolayer dispersion, does not modify qualitatively the features found in

twisted bilayer graphene.

To summarize, our main results are:

- The long-range electron-electron interaction modifies significantly the central bands. The Hartree potential widens the bands, leading to a bandwidth $\sim 20-40$ meV. The exchange potential at half filling separates the occupied valence band from the empty conduction band, which become $20-40$ meV apart. The presence of an additional linearly dispersive band prevents the formation of a gap and an insulating state.

- Long-wavelength charge fluctuations, renormalized by their coupling by the electrostatic interaction, and also by their interaction with longitudinal acoustic phonons, are sufficient to induce superconductivity, with critical temperatures up to a few Kelvin. The order parameter has a significant structure near the Fermi surface pockets. Pairing by long-wavelength excitations, which do not mix valleys, leads to degenerate spin singlet/valley triplet and spin triplet/valley singlet superconducting phases.

Acknowledgements. This work was supported by funding from the European Commision, under the Graphene Flagship, Core 3, grant number 881603, and by the grants NMAT2D (Comunidad de Madrid, Spain), SprQuMat and SEV-2016-0686, (Ministerio de Ciencia e Innovacin, Spain). VTP acknowledges support from the NSF Graduate Research Fellowships Program and the P.D. Soros Fellowship for New Americans.

[1] Y. Cao, V. Fatemi, A. Demir, S. Fang, S. L. Tomarken, J. Y. Luo, J. D. Sanchez-Yamagishi, K. Watanabe, T. Taniguchi, E. Kaxiras, R. C. Ashoori, and P. Jarillo-Herrero, Correlated insulator behaviour at half-filling in magic-angle graphene superlattices, Nature **556**, 80 (2018), arXiv:1802.00553.

[2] Y. Cao, V. Fatemi, S. Fang, K. Watanabe, T. Taniguchi, E. Kaxiras, and P. Jarillo-Herrero, Unconventional superconductivity in magic-angle graphene superlattices, Nature **556**, 43 (2018).

[3] J. M. Park, Y. Cao, K. Watanabe, T. Taniguchi, and P. Jarillo-Herrero, Tunable strongly coupled superconductivity in magic-angle twisted trilayer graphene, Nature **590**, 249 (2021).

[4] Z. Hao, A. M. Zimmerman, P. Ledwith, E. Khalaf, D. H. Najafabadi, K. Watanabe, T. Taniguchi, A. Vishwanath, and P. Kim, Electric fieldtunable superconductivity in alternating-twist magic-angle trilayer graphene, Science **371**, 1133 (2021).

[5] S. Moriyama, Y. Morita, K. Komatsu, K. Endo, T. Iwasaki, S. Nakaharai, Y. Noguchi, Y. Wakayama, E. Watanabe, D. Tsuya, K. Watanabe, and T. Taniguchi, Observation of superconductivity in bilayer graphene/hexagonal boron nitride superlattices, arXiv e-prints , arXiv:1901.09356 (2019), arXiv:1901.09356 [cond-mat.supr-con].

[6] C. Shen, Y. Chu, Q. Wu, N. Li, S. Wang, Y. Zhao, J. Tang, J. Liu, J. Tian, K. Watanabe, T. Taniguchi, R. Yang, Z. Y. Meng, D. Shi, O. V. Yazyev, and G. Zhang, Correlated states in twisted double bilayer graphene, Nature Physics **16**, 520 (2020).

[7] G. Chen, A. L. Sharpe, P. Gallagher, I. T. Rosen, E. J. Fox, L. Jiang, B. Lyu, H. Li, K. Watanabe, T. Taniguchi, J. Jung, Z. Shi, D. Goldhaber-Gordon, Y. Zhang, and F. Wang, Signatures of tunable superconductivity in a trilayer graphene moiré superlattice, Nature **572**, 215 (2019), arXiv:1901.04621.

[8] G. Chen, L. Jiang, S. Wu, B. Lyu, H. Li, B. L. Chittari, K. Watanabe, T. Taniguchi, Z. Shi, J. Jung, Y. Zhang, and F. Wang, Evidence of a gate-tunable Mott insulator in a trilayer graphene moiré superlattice, *Nature Physics*, **15**, 237 (2019).

[9] G. Chen, A. L. Sharpe, E. J. Fox, Y.-H. Zhang, S. Wang, L. Jiang, B. Lyu, H. Li, K. Watanabe, T. Taniguchi, Z. Shi, T. Senthil, D. Goldhaber-Gordon, Y. Zhang, and F. Wang, Tunable correlated chern insulator and ferromagnetism in a moirésuperlattice, Nature **579**, 56 (2020).

[10] B. L. Chittari, G. Chen, Y. Zhang, F. Wang, and J. Jung, Gate-Tunable Topological Flat Bands in Trilayer Graphene Boron-Nitride Moiré Superlattices, Physical Review Letters **122**, 016401 (2019), arXiv:1806.00462.

[11] M. He, Y. Li, J. Cai, Y. Liu, K. Watanabe, T. Taniguchi, X. Xu, and M. Yankowitz, Symmetry breaking in twisted double bilayer graphene, Nature Physics **17**, 26 (2021).

[12] X. Liu, Z. Hao, E. Khalaf, J. Y. Lee, Y. Ronen, H. Yoo, D. Haei Najafabadi, K. Watanabe, T. Taniguchi, A. Vishwanath, and P. Kim, Tunable spin-polarized correlated states in twisted double bilayer graphene, Nature **583**, 221 (2020).

[13] Y. Cao, D. Rodan-Legrain, O. Rubies-Bigorda, J. M. Park, K. Watanabe, T. Taniguchi, and P. Jarillo-Herrero, Tunable correlated states and spin-polarized phases in twisted bilayer–bilayer graphene, Nature **583**, 215 (2020).

[14] K.-T. Tsai, X. Zhang, Z. Zhu, Y. Luo, S. Carr, M. Luskin, E. Kaxiras, and K. Wang, Correlated Insulating States and Transport Signature of Superconductivity in Twisted Trilayer Graphene Moiré of Moiré Superlattices, arXiv e-prints , arXiv:1912.03375 (2019), arXiv:1912.03375 [cond-mat.mes-hall].

[15] A. Kerelsky, C. Rubio-Verdú, L. Xian, D. M. Kennes, D. Halbertal, N. Finney, L. Song, S. Turkel, L. Wang, K. Watanabe, T. Taniguchi, J. Hone, C. Dean, D. Basov, A. Rubio, and A. N. Pasupathy, Moiré-less Correlations in ABCA Graphene, arXiv e-prints , arXiv:1911.00007 (2019), arXiv:1911.00007 [cond-mat.mes-hall].

[16] H. Zhou, T. Xie, A. Ghazaryan, T. Holder, J. R. Ehrets, E. M. Spanton, T. Taniguchi, K. Watanabe, E. Berg, M. Serbyn, and A. F. Young, Half and quarter metals in rhombohedral trilayer graphene, arXiv e-prints , arXiv:2104.00653 (2021), arXiv:2104.00653 [cond-mat.mes-hall].

[17] H. Zhou, T. Xie, T. Taniguchi, K. Watanabe, and A. F. Young, Superconductivity in rhombohedral trilayer graphene, arXiv e-prints , arXiv:2106.07640 (2021), arXiv:2106.07640 [cond-mat.mes-hall].

[18] L. Wang, E.-M. Shih, A. Ghiotto, L. Xian, D. A. Rhodes, C. Tan, M. Claassen, D. M. Kennes, Y. Bai, B. Kim,

K. Watanabe, T. Taniguchi, X. Zhu, J. Hone, A. Rubio, A. N. Pasupathy, and C. R. Dean, Correlated electronic phases in twisted bilayer transition metal dichalcogenides, Nature Materials **19**, 861 (2020).
[19] X. Lu, P. Stepanov, W. Yang, M. Xie, M. A. Aamir, I. Das, C. Urgell, K. Watanabe, T. Taniguchi, G. Zhang, A. Bachtold, A. H. MacDonald, and D. K. Efetov, Superconductors, orbital magnets and correlated states in magic-angle bilayer graphene, Nature **574**, 653 (2019).
[20] H. S. Arora, R. Polski, Y. Zhang, A. Thomson, Y. Choi, H. Kim, Z. Lin, I. Z. Wilson, X. Xu, J.-H. Chu, K. Watanabe, T. Taniguchi, J. Alicea, and S. Nadj-Perge, Superconductivity in metallic twisted bilayer graphene stabilized by wse2, Nature **583**, 379 (2020).
[21] M. Yankowitz, S. Chen, H. Polshyn, Y. Zhang, K. Watanabe, T. Taniguchi, D. Graf, A. F. Young, and C. R. Dean, Tuning superconductivity in twisted bilayer graphene, Science **363**, 1059 (2019), https://science.sciencemag.org/content/363/6431/1059.full.pdf.
[22] E. Khalaf, A. J. Kruchkov, G. Tarnopolsky, and A. Vishwanath, Magic angle hierarchy in twisted graphene multilayers, Phys. Rev. B **100**, 085109 (2019).
[23] Z. Wu, Z. Zhan, and S. Yuan, Lattice relaxation, mirror symmetry and magnetic field effects on ultraflat bands in twisted trilayer graphene, Science China Physics, Mechanics & Astronomy **64**, 267811 (2021).
[24] A. Ramires and J. L. Lado, Emulating heavy fermions in twisted trilayer graphene, Phys. Rev. Lett. **127**, 026401 (2021).
[25] D. Călugăru, F. Xie, Z.-D. Song, B. Lian, N. Regnault, and B. A. Bernevig, Twisted symmetric trilayer graphene: Single-particle and many-body hamiltonians and hidden nonlocal symmetries of trilayer moiré systems with and without displacement field, Phys. Rev. B **103**, 195411 (2021).
[26] J. Shin, B. Lingam Chittari, and J. Jung, Stacking and gate tunable topological flat bands, gaps and anisotropic strip patterns in twisted trilayer graphene, arXiv e-prints , arXiv:2104.01570 (2021), arXiv:2104.01570 [cond-mat.mes-hall].
[27] A. Fischer, Z. A. H. Goodwin, A. A. Mostofi, J. Lischner, D. M. Kennes, and L. Klebl, Unconventional Superconductivity in Magic-Angle Twisted Trilayer Graphene, arXiv e-prints , arXiv:2104.10176 (2021), arXiv:2104.10176 [cond-mat.supr-con].
[28] E. Lake and T. Senthil, Re-entrant superconductivity through a quantum lifshitz transition in twisted trilayer graphene, (2021), arXiv:2104.13920 [cond-mat.mes-hall].
[29] Z. A. H. Goodwin, L. Klebl, V. Vitale, X. Liang, V. Gogtay, D. M. K. Xavier van Gorp, A. A. Mostofi, and J. Lischner, Flat bands, electron interactions and magnetic order in magic-angle mono-trilayer graphene, (2021), arXiv:2105.12641 [cond-mat.mes-hall].
[30] M. Christos, S. Sachdev, and M. S. Scheurer, Correlated insulators, semimetals, and superconductivity in twisted trilayer graphene, (2021), arXiv:2106.02063 [cond-mat.mes-hall].
[31] Y.-Z. Chou, F. Wu, J. D. Sau, and S. Das Sarma, Correlation-induced triplet pairing superconductivity in graphene-based moiré systems, arXiv e-prints , arXiv:2105.00561 (2021), arXiv:2105.00561 [cond-mat.supr-con].
[32] W. Qin and A. H. MacDonald, In-plane critical magnetic fields in magic-angle twisted trilayer graphene, (2021), arXiv:2104.14026 [cond-mat.mes-hall].
[33] R. Bistritzer and A. H. MacDonald, Moiré bands in twisted double-layer graphene, Proceedings of the National Academy of Sciences **108**, 12233 (2011), https://www.pnas.org/content/108/30/12233.full.pdf.
[34] M. Koshino, N. F. Q. Yuan, T. Koretsune, M. Ochi, K. Kuroki, and L. Fu, Maximally localized wannier orbitals and the extended hubbard model for twisted bilayer graphene, Phys. Rev. X **8**, 031087 (2018).
[35] X. Li, F. Wu, and A. H. MacDonald, Electronic Structure of Single-Twist Trilayer Graphene, arXiv e-prints , arXiv:1907.12338 (2019), arXiv:1907.12338 [cond-mat.mtrl-sci].
[36] J. W. McClure, Band structure of graphite and de haas-van alphen effect, Phys. Rev. **108**, 612 (1957).
[37] J. C. Slonczewski and P. R. Weiss, Band structure of graphite, Phys. Rev. **109**, 272 (1958).
[38] T. Cea, P. A. Pantaleón, and F. Guinea, Band structure of twisted bilayer graphene on hexagonal boron nitride, Phys. Rev. B **102**, 155136 (2020).
[39] J. Shi, J. Zhu, and A. H. MacDonald, Moiré commensurability and the quantum anomalous hall effect in twisted bilayer graphene on hexagonal boron nitride, Phys. Rev. B **103**, 075122 (2021).
[40] J. Shin, Y. Park, B. L. Chittari, J.-H. Sun, and J. Jung, Electron-hole asymmetry and band gaps of commensurate double moire patterns in twisted bilayer graphene on hexagonal boron nitride, Phys. Rev. B **103**, 075423 (2021).
[41] D. Mao and T. Senthil, Quasiperiodicity, band topology, and moiré graphene, Phys. Rev. B **103**, 115110 (2021).
[42] X. Lin, K. Su, and J. Ni, Misalignment instability in magic-angle twisted bilayer graphene on hexagonal boron nitride, 2D Materials **8**, 025025 (2021).
[43] L. Zou, H. C. Po, A. Vishwanath, and T. Senthil, Band structure of twisted bilayer graphene: Emergent symmetries, commensurate approximants, and wannier obstructions, Phys. Rev. B **98**, 085435 (2018).
[44] Z. Song, Z. Wang, W. Shi, G. Li, C. Fang, and B. A. Bernevig, All magic angles in twisted bilayer graphene are topological, Phys. Rev. Lett. **123**, 036401 (2019).
[45] See Supplementary material.
[46] F. Guinea and N. R. Walet, Electrostatic effects, band distortions, and superconductivity in twisted graphene bilayers, Proceedings of the National Academy of Sciences 10.1073/pnas.1810947115 (2018), https://www.pnas.org/content/early/2018/12/10/1810947115.full.pd
[47] T. Cea, N. R. Walet, and F. Guinea, Electronic band structure and pinning of Fermi energy to Van Hove singularities in twisted bilayer graphene: A self-consistent approach, Physical Review B **100**, 205113 (2019), arXiv:1906.10570.
[48] T. Cea and F. Guinea, Band structure and insulating states driven by Coulomb interaction in twisted bilayer graphene, Physical Review B **102**, 045107 (2020), arXiv:2004.01577.
[49] We assume that the initial hoppings include the renormalization due to the exchange potential from the bands other than the sisx central bands, so that no substraction of the exchange potential is required.
[50] T. Cea and F. Guinea, Coulomb interaction, phonons, and superconductivity in twisted bilayer graphene, arXiv e-prints , arXiv:2103.01815 (2021), arXiv:2103.01815 [cond-mat.str-el].

[51] W. Kohn and J. M. Luttinger, New mechanism for superconductivity, Phys. Rev. Lett. **15**, 524 (1965).
[52] Y. Cao, J. M. Park, K. Watanabe, T. Taniguchi, and P. Jarillo-Herrero, Large Pauli Limit Violation and Reentrant Superconductivity in Magic-Angle Twisted Trilayer Graphene, arXiv e-prints , arXiv:2103.12083 (2021), arXiv:2103.12083 [cond-mat.mes-hall].